A Single-step Process towards Achieving Superhydrophobic Reduced Graphene Oxide

Zhong Li,[†] Xiu-Zhi Tang,[†] Zhu Wenyu,[‡] Brianna C. Thompson,[†] Mingyue Huang,[†] Jinglei Yang,[†] Xiao Hu,[§] and Khiam Aik Khor [, †]*

[†]School of Mechanical & Aerospace Engineering, Nanyang Technological University, 50 Nanyang Avenue, Singapore 639798. E-mail: mkakhor@ntu.edu.sg.

[‡]School of Civil & Environmental Engineering, Nanyang Technological University, 50 Nanyang Avenue, Singapore 639798

[§]School of Materials Science & Engineering, Nanyang Technological University, 50 Nanyang Avenue, Singapore 639798

KEYWORDS: graphene oxide, thermal reduction, spark plasma sintering, superhydrophobicity, antibacterial nanomaterials

ABSTRACT: We report the first use of Spark Plasma Sintering (SPS) as a single-step process to achieve superhydrophobic reduced graphene oxide (rGO). It was found that SPS was capable of converting smooth and electrically insulating graphene oxide (GO) sheets into highly electrically conductive rGO with minimum residual oxygen and hierarchical roughness which could be well retained after prolonged ultrasonication. At a temperature of 500 °C, which is lower than the conventional critical temperature for GO exfoliation, GO was successfully exfoliated, reduced and hierarchically roughened. rGO fabricated by only 1 min treatment at 1050 °C was superhydrophobic with a surface roughness (R_a) 10 times as big as GO as well as an extraordinarily high C:O ratio of 83.03 (at.%) and water contact angle of 153°. This demonstrates that SPS is a superior GO reduction technique, which enabled superhydrophobic rGO to be quickly and effectively achieved in one single step. Moreover, the superhydrophobic rGO fabricated by SPS showed impressive bacterial antifouling and inactivation effect against *Escherichia coli* in both aqueous solution and solid state. It is envisioned that the superhydrophobic rGO obtained in this study can be potentially used for a wide range of industrial and biomedical applications such as the fabrication of self-cleaning and antibacterial surfaces.

1. INTRODUCTION

Graphene is a fascinating 2D nanomaterial with exceptional electronic, mechanical, optical and thermal properties.[1-3] Due to the difficulty in large-scale fabrication of pristine graphene, graphene oxide (GO) is one of the major precursors to graphene-based applications.[4-6] The numerous similarities between reduced graphene oxide (rGO) and pristine graphene have made the reduction of GO one of its most important reactions.[7-11]

Compared with chemical reduction which usually involves the use of hazardous reagents and requires post-reduction purification,[12-13] thermal reduction of GO is an efficient and convenient high-yield process. Thermal reduction of GO is typically conducted by briefly inserting a quartz tube filled with GO and flushed with inert gas into a furnace preheated to 1050 °C with a typical heating period of 30 seconds.[5, 14-15] Besides strict safety precautions that have to be taken, such processes suffer from poor repeatability caused by varying inert gas concentration in the quartz tube, unknown real-time temperature in the furnace, and uncontrollable speed of quartz tube insertion. Thermal reduction processes with improved feasibility and repeatability are thus warranted.

Spark Plasma Sintering (SPS) has emerged as an advanced materials processing technique which has been utilized to develop a wide variety of structural and functional materials.[16-18] In the SPS process, pulsed DC flows through both the die and the sample and generates spark plasma within the sample.[19-20] The sample was thus subjected simultaneously to a high electric field treatment and heated internally by Joule heating and externally by spark plasma and heat transferred from the die and punches. Several unique characteristics of SPS solidify its great potential in the thermal reduction of GO: (1) it can offer a heating rate as high as 2000 °C/min,[21] which is desirable in conventional thermal reduction processes; (2) the process is conducted in vacuum (~5 Pa), meaning that GO can be protected from reacting with air at high temperatures; (3) GO is sealed in a graphite die-punch combination, which minimizes contamination and sample loss; and (4) the generated spark and plasma[22] and the high temperature can possibly result in a synergetic effect to minimize residual oxygen-containing functional groups and achieve high reduction degree of rGO. It has been reported that GO could be reduced *in situ* when SPS was used to fabricate rGO-ceramic composites with matrixes such as silica[23] and

silicon nitride[24-25]. However, there has been no systematic investigations into the reduction of GO by SPS to date.

Superhydrophobic surfaces (with water contact angle (CA) larger than 150°) have found many intriguing applications such as self-cleaning surfaces and antifouling coatings.[26-28] Two important factors contributing to the realization of superhydrophobicity are: (1) a material with low surface energy, and (2) hierarchically rough surface microstructure.[29] To this end, research efforts have been dedicated to two major areas: (1) decreasing the surface energy of graphene and rGO by various methods such as chemical modification,[28] and (2) enhancing surface roughness by either roughening the graphene/rGO surface or coating graphene/rGO sheets onto rough scaffolds or substrates.[26, 30-31] To date the two purposes have been realized by two separate processes in most studies. It is believed that a single process capable of achieving both outcomes will lower the fabrication cost and improve the scalability of graphene-based superhydrophobic surfaces.

When interacting with bacterial cells, a number of superhydrophobic coatings have demonstrated plausible antifouling and/or antibacterial properties.[32-34] The intrinsic hydrophobicity of graphene and rGO means that they have potential in the fabrication of superhydrophobic surfaces and may be utilized to achieve antibacterial effects. It has been reported that rGO nanowalls were more toxic to bacteria than the GO ones due to their sharper edges and the better charge transfer between bacteria and rGO nanowalls.[35] By comparing the antibacterial activity of different graphene-based materials, Liu et al. found that conductive rGO could impose higher oxidative stresses on bacterium cells than insulating GO.[36] In addition, Hu et al. reported that compared with GO, the cytotoxicity of rGO was significantly higher, although

their antibacterial properties was slightly lower.[37] Nevertheless, the antifouling and antibacterial effects of superhydrophobic rGO have been much less studied.

In this study, SPS, which can overcome the aforementioned drawbacks of conventional thermal reduction processes, is reported for the first time as a facile single-step process to fabricate superhydrophobic rGO. SPS-reduced GO (SPSrGO) treated at 1050 °C for only 1 min demonstrated a water CA as high as 153° due to minimal residual oxygen and hierarchical roughness in both micro- and nano-scale. Furthermore, the superhydrophobic SPSrGO also showed excellent bacterial antifouling and inactivation properties when tested with *Escherichia coli* (*E. coli*) due to its hierarchical roughness and high electrical conductivity.

2. EXPERIMENTAL SECTION

2.1. GO Reduction by SPS. GO was synthesized from natural graphite flakes using a modified Hummers method.[38-39] 0.24 g freeze-dried GO powder was loaded into a graphite die with an inner diameter of 20 mm and clamped between two graphite punches. All the reduction processes were conducted by holding the GO sample in an SPS system (Dr. Sinter 1050, Sumitomo Coal Mining, Japan) at preset temperatures for 1 min, unless otherwise specified. A schematic of the SPS setup used is given in Fig. 1. Heating and cooling rates were both set to be 100 °C min^{-1}. Sample names and the corresponding SPS parameters are summarized in Table 1. Temperature measurement was realized by an infrared pyrometer focused on a 2 mm hole on the graphite die, or when the highest temperature was < 600 °C, a thermal couple inserted into the hole.

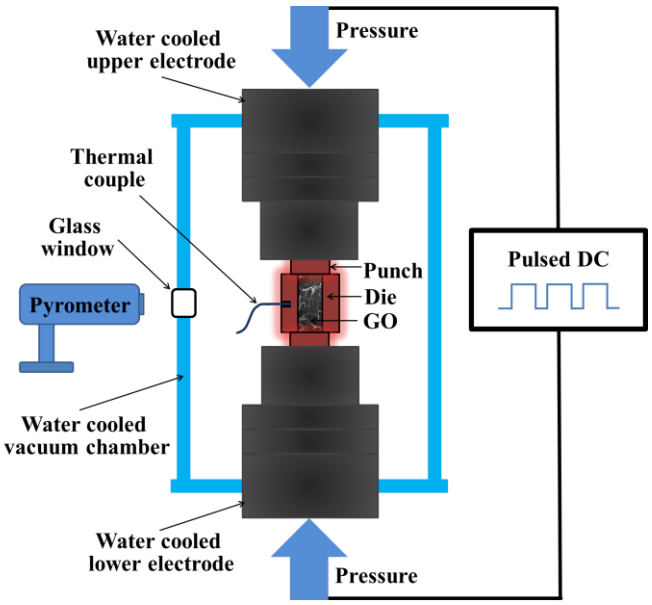

Fig. 1. Schematic of the setup for reducing GO by SPS.

Table 1. Processing parameters and properties of GO and SPSrGO samples [a]

Sample name	Processing parameters	C:O ratios (by at. %/ wt. %)	BET surface area (m^2/g)	Interlamellar spacing (Å)	I_D/I_G ratio	Buckypaper sheet resistance (Ω/sq.)
GO	N.A.	2.26/1.70	83	8.07	0.85	$> 2 \times 10^6$
SPSrGO-500	500-1-1	9.62/7.22	734	3.56	0.80	12.4 ± 0.8
SPSrGO-900	900-1-1	82.33/61.89	806	3.55	0.91	1.77 ± 0.05
SPSrGO-1050	1050-1-1	83.03/62.69	859	3.57	1.05	1.85 ± 0.03
SPSrGO-2C500	500-1-2	15.13/11.35	818	3.42	0.74	13.61 ± 0.04
SPSrGO-3C500	500-1-3	14.90/11.18	1266	3.43	0.76	17 ± 1
SPSrGO-500E	500-3-1	11.71/8.78	800	3.40	0.79	14.0 ± 0.2

[a] Processing parameters: highest temperature (°C) – holding time (min) – No. of processing cycles; I_D/I_G ratio calculated from Raman spectra; C:O ratios were determined from the XPS

detail scan spectra; Interlamellar spacing calculated from XRD patterns; buckypaper sheet resistance data given as average ± standard deviation; sheet resistance of GO could not be obtained as it exceeded the measuring range (1 mΩ/sq. to 2 MΩ/sq.) of the four-point probe.

In order to elucidate the role of spark and plasma generated during the heating up stage in reducing the GO, two samples, denoted as SPSrGO-2C500 and SPSrGO-3C500, were fabricated with the number of processing (i.e., heating-holding-cooling) cycles being 2 and 3, respectively, using 500 °C as the highest temperature. For comparison SPSrGO-500E was also fabricated by holding at 500 °C for an extended duration of 3 min in one processing cycle.

2.2. Characterization. The chemical state of C and O in GO and SPSrGO samples was investigated by X-ray photoelectron spectroscopy (XPS, Kratos, Axis-ULTRA, UK) equipped with an Al Kα (1486.6 eV) monochromatic X-ray source. Thermal stability of the GO and SPSrGO samples was investigated by Thermal Gravimetric Analysis (TGA, TA Instruments Q500, US) using a heating rate of 10 °C min^{-1}. Specific surface area of the powders was determined by a gas sorption analyzer based on the Brunauer-Emmett-Teller (BET) method, using a QuadraSorb Station 2 Surface Area and Pore Size Analyzer (Quantachrome Instruments, US). Crystallinity of the SPSrGO samples was tested using an X-ray Diffractometer (XRD, Philips MPD 1880 diffractometer, The Netherlands) at 0.01 ° s^{-1} with a Cu Kα radiation. Fourier Transform Infrared Spectroscopy (FTIR, PerkinElmer Frontier) was used to compare the functional groups in GO and SPSrGO powders. Raman spectra of GO and SPSrGO samples were collected using a Rapid Imaging Micro-Raman Spectrophotometer System (Renishaw Invia, UK) with a 488 nm line of HeNe laser. Sheet resistance of GO and SPSrGO buckypaper prepared with a hydraulic press was measured by a four-point probe (CMT-SR2000NW, Materials Development Corporation, US) and averaged from 6 measurements.

Morphology of the samples was observed using both Transmission Electron Microscope (TEM, JEOL JEM 2010, Japan) and Field Emission Scanning Electron Microscope (FESEM, JEOL JSM 7600F, Japan). Atomic Force Microscope (AFM, Park Systems, Suwon, South Korea) imaging was conducted in ambient environment to obtain topographic and phase images of the samples as well as to determine the thickness of the GO sheets.

2.3. Wettability and Antibacterial Tests. GO and SPSrGO were dispersed at a concentration of 1 mg mL^{-1} in DI water and dimethylformamide (DMF), respectively. 1 mL of both solutions was then used to cast a coating on parafilm for hydrophobicity tests. An Attension Theta Optical Tensiometer (Biolin Scientific, Sweden) was used to obtain the water contact angle.

Using *E. coli* (ATCC 8739) as the model bacterium, bacterial attachment and growth on GO and SPSrGO-1050 were investigated with two different culture media. Firstly, the bacterial cell culture was conducted in aqueous conditions. GO and SPSrGO-1050 were dispersed at 50 μg mL^{-1} in 0.85% saline solution by ultrasonication. After *E. coli* cells (~10^7 colony forming units) were added into both solutions, they were incubated at 37 °C for 2 h, during which the incubator bed kept shaking at 250 rpm to ensure homogeneous dispersion of GO and SPSrGO-1050 in the saline solution during the entire incubation process. For comparison purposes *E. coli* was also cultured in 0.85% pure saline solution under the same conditions. After incubation the solutions were dropped onto Si wafer and dried at 37 °C for FESEM studies.

Moreover, we further studied the possible antibacterial effect of filtered GO and SPSrGO-1050 coatings. 600 μL of sonicated GO/DMF and SPSrGO-1050/DMF solution (1 mg mL^{-1}) was carefully dropped onto 0.1 μm Teflon filters. The same amount of pure DMF was dropped onto a

Teflon filter as control. The filters had been left to dry in the fume hood for 12 h before they were treated overnight in a 60° oven to fully remove the residual DMF. These filters were then carefully put onto solid Luria-Bertani nutrient agar plates with newly inoculated *E. coli*. The agar plates were incubated at 37°C for 18 h after which the coated filters were carefully removed for FESEM observation.

3. RESULTS AND DISCUSSION

3.1. Chemical Composition and Structural Characteristics. Fig. 2 shows the XPS survey and C 1s detail scan spectra for GO and SPSrGO-1050. Only peaks corresponding to C and O were present in the spectra (Fig. 2a), demonstrating no contamination from other elements. It can be seen that SPSrGO samples all showed enhanced C 1s peak and weakened O 1s peak as compared to GO, and this phenomenon was more obvious as reduction temperature increased. To quantify the change in the relative intensity of those two peaks, we calculated each sample's C:O ratio, which has been widely used to indicate the extent of reduction for rGO where a higher value means elimination of more oxygen-containing functional groups and greater extent of reduction. As shown in Fig. 2b and Table 1, GO has a low C:O ratio of 2.26 (by at.%). This value was improved by over 4 times to 9.62 for SPSrGO-500. Most excitingly, SPSrGO900 and SPSrGO-1050 achieve an extraordinarily high C:O ratio of 82.33 and 83.03, respectively, corresponding to more than 30-fold increase as compared with GO. Such a high C:O ratio has rarely been reported for rGO, and to the best of our knowledge, this is the highest value achieved for thermally reduced rGO thus far (Table S1). It is worth mentioning that although an even higher value was reported by Gao *et al.*,[4] a complex chemical reduction process was used in conjunction with thermal annealing at 1100 °C.

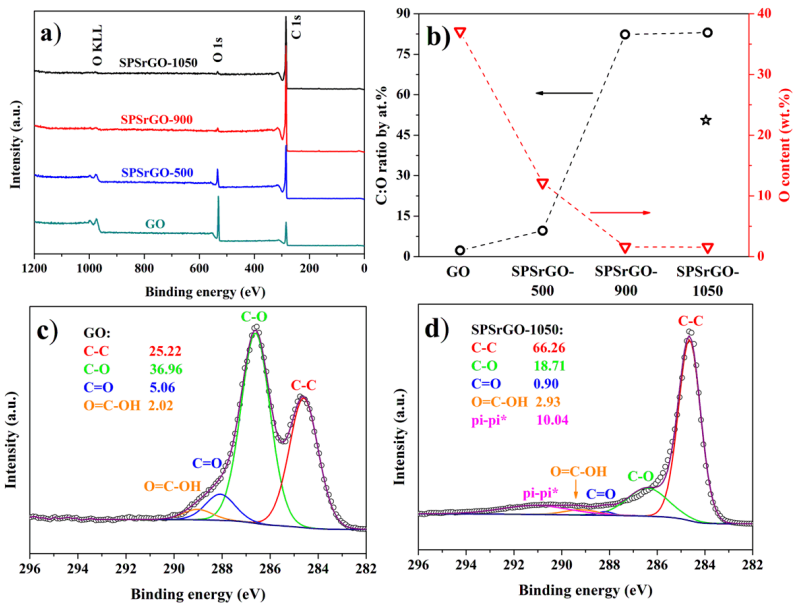

Fig. 2. (a, c, d) XPS spectra of GO and SPSrGO: survey scan spectra (a), and C 1s spectrum of GO (c) and SPSrGO-1050 (d), where the purple line stands for fitted envelops and open circle for measured data and numbers denote at.% of major deconvoluted components; (b) C:O ratios and O content (wt %) in GO and SPSrGO, where the star represents C:O ratio from Ref [40] where rGO was fabricated by conventional thermal reduction at 400 °C for 30 min followed by 1200 °C for 30 min.

Fig. 2c and d shows the as-obtained and deconvoluted C1s detail-scan spectra for GO and SPSrGO-1050. A C-O component stronger than the C-C one was seen for GO, together with two other components corresponding to C=O and O=C-OH. This proves the existence of a large quantity of oxygen-containing groups. The C-O component intensity was significantly decreased in SPSrGO-1050, and correspondingly, C-C component obviously intensified. In addition, after the SPS process one new component located at ~291.2 eV appeared, which was the shake-up satellite (pi-pi* bonding) stemming from the aromatic character of graphene. This distinct pi-pi*

bonding was also observed in SPSrGO-500 and PSrGO-900 (Figure S1), and it clearly demonstrates the restoration of the conjugated network that did not exist in GO.

The structural characteristics of SPSrGO were extensively characterized by TGA, XRD, selected area electron diffraction (SAED), FTIR, Raman spectroscopy, and BET surface area measurement. SPSrGO-500, SPSrGO-900 and SPSrGO-1050 all showed significantly higher thermal stability and surface area than GO (Figure S2 and Table 1). Interestingly, it has been reported that a critical temperature of 550 °C has to be exceeded for GO to be thermally exfoliated.[14] Nevertheless, it is clearly seen in the current study that a lower SPS temperature of 500 °C could effectively exfoliate GO. SPS thus appears to be a superior thermal treatment procedure for GO exfoliation and reduction. XRD patterns shown in Figure S3 clearly signified decreased crystallinity in SPSrGO, which is supported by the TEM SAED patterns (Fig. 3c and d insets). A typical sharp polycrystalline ring pattern was observed for GO, while diffuse and weak rings without any bright spots were seen for SPSrGO-1050. The calculated interlamellar spacing (Table 1) decreased from 8.07 Å for GO to 3.4-3.6 Å for SPSrGO, mainly due to the decomposition of oxygen containing groups and their associated structural defects as well as the evaporation of intercalated water. FTIR spectra showed significantly suppressed absorption peaks for C=O carboxyl/carbonyl and C-O epoxy in all SPSrGO samples (Figure S4), indicating that most of those groups had been removed in the SPS process. Peaks corresponding to the D and G band were explicitly seen at ~1357 and ~1595 cm^{-1}, respectively, in Raman spectra of GO and SPSrGO (Figure S5). In addition, it was found that all SPSrGO samples reduced at 500 °C had decreased I_D/I_G (defect index: intensity ratio of the D band and G band) compared with GO. This could be attributed to the removal of oxygen-containing functional groups and restoration of sp^2 bonds in the graphite lattice.[40] On the contrary, SPSrGO samples reduced at above 500 °C

showed I_D/I_G higher than that of GO. This was probably caused by an increased number of structural defects induced at higher temperatures due to the generation of more intense spark and plasma. It is worth mentioning that the SPSrGO-900 and SPSrGO-1050 still showed remarkably lower sheet resistance than SPSrGO treated at 500 ℃ (Table 1). As evidenced by the much higher C:O ratios, both 900 ℃ and 1050 ℃ could enable a significantly higher number of oxygen containing groups to be removed than 500 ℃, although the I_D/I_G values imply that more SPS-induced structural defects would probably be introduced at those temperatures. The much higher reduction degree should be the main contributor to the lower sheet resistance of SPSrGO reduced at above 500 ℃. SPSrGO-900 demonstrated a notably high electrical conductivity of 1564 ± 40 S/m, which is higher or comparable to those from other thermal processes (Table S1).[4, 14-15, 41] It has been reported previously that I_D/I_G was only observed to decrease with thermal annealing temperature higher than 1000 °C.[40] Our results further confirm the superior effectiveness of SPS in restoring sp^2 carbon-carbon bonds as it enabled a decreased I_D/I_G to be achieved at a low temperature of 500 °C.

3.2. Morphological Characteristics and Underlying Mechanisms. Fig. 3 shows the FESEM and TEM images of dried GO and SPSrGO-1050 after brief bath sonication in ethanol. While GO sheets were smooth, SPSrGO samples were characterized by micro-scale sheet bending as well as submicron or nano-sized rough structures. Similar hierarchically rough morphology was also seen for SPSrGO-500 and SPSrGO-900 (Figure S6). In addition, when dispersed in DI water by sonication and dropped onto Si wafer, GO sheets were able to stretch out and overlap each other, whereas SPSrGO demonstrated an agglomerated and granular appearance (Figure S7). In TEM images (Fig. 3c and d), the morphology of GO also contrasted dramatically with that of SPSrGO-1050. While GO presented very smooth sheets, SPSrGO-1050

was wrinkled and corrugated with both micro- and nano-sized structures. The drastic difference in topography between GO and SPSrGO-1050 was also obvious under Atomic Force Microscope (AFM, see Figure S8). GO sheets tend to spread and adhere to the silicon substrate, with the majority of their surface being flat and smooth. On the contrary, SPSrGO-1050 showed a much rougher surface with numerous micron and submicron scale protrusions. The surface roughness (R_a) was obtained from three 0.5 μm × 0.5 μm regions randomly selected in Figure S8a and b. It was found that the average R_a for SPSrGO-1050 (19 ± 4 nm) was increased by a factor of ~10 compared with that of GO (1.9 ± 0.3 nm). The height profile was recorded for one GO sheet (Figure S8g) and gave an average sheet thickness of ~2 nm which is typical for few-layer GO sheets. The FESEM, TEM and AFM results confirm that SPS induced the formation of hierarchical surface roughness in the SPSrGO samples.

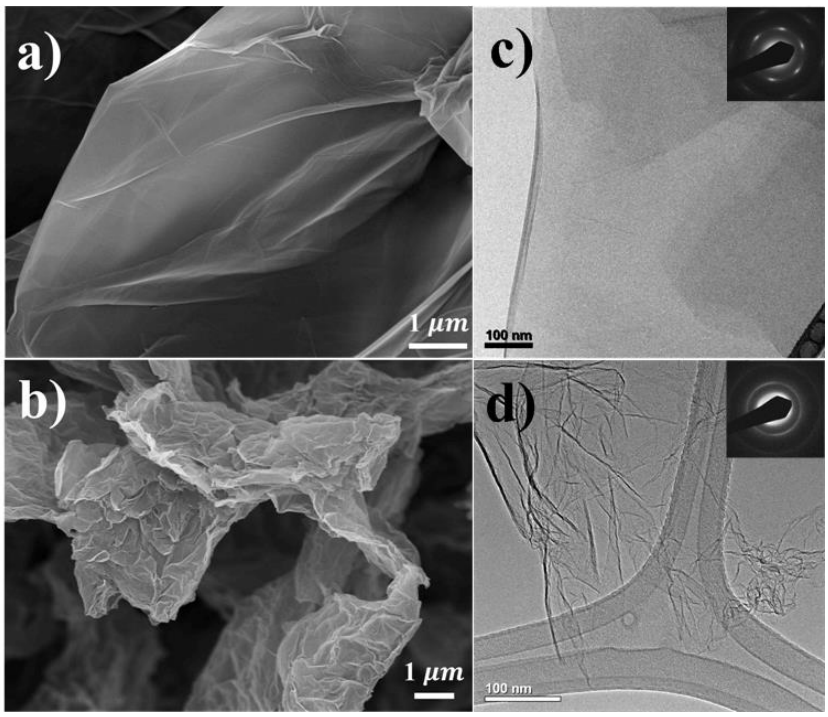

Fig. 3. FESEM (a, b) and TEM (c, d) images of GO (a, c) and SPSrGO-1050 (b, d). SAED patterns are shown in the inserts of (c, d).

Wrinkled structures in rGO thermally treated by a tube furnace have also been observed.[14-15] However, in the previous studies the corrugated appearance could no longer be retained after dispersing the rGO sample by sonication,[14] while in the current study it remains well preserved. Consideration is thus directed to the unique characteristics of the SPS process, which are the major differences between our thermal reduction route and the previously reported ones. It has long been recognized that the application of pulsed DC grants SPS a number of advantages over conventional sintering techniques, such as generation of speak and plasma, high-density energy supply and local high temperature.[21, 42] In our previous studies SPS has been applied as an effective heat treatment technique.[17, 43] This idea was also adopted by Cao *et al*.[44] who processed rGO by SPS at 1300 °C for 5 min. It was found that SPS induced the formation of many ripples which changed smooth rGO surfaces into rough ones. They proposed that on rGO surfaces there exist high/low regions with a larger electronic density which are susceptible to discharge and plasma striking during the SPS process. Unlike this previous work, in the current study smooth GO sheets were directly treated by SPS with no prior heating/reduction. GO reduction and ripple formation thus occurred simultaneously. It is interesting to note that in the study by Cao *et al*. ,[44] GO sheets thermally reduced by conventional method at 700 °C for 2 h were still very smooth while in our study SPSrGO-500 already showed obvious hierarchical surface roughness. This further confirms the superiority of SPS in inducing rough rGO surfaces.

Because of the low density of freeze-dried GO, the 0.24 g GO clusters used in all SPS experiments were in good contact with other GO flakes as well as with the graphite die and punches. During SPS, electric current flows through both the graphite die and GO powder, with the majority of current likely flowing through the die due to its higher conductivity. Current flow results in joule heating from both the die and the GO powder leading to uniform heating across

the whole sample. SPS has been well known to result in surface purification and activation due to the spark plasma.[42] In our study, the spark plasma likely contributes to the cleaving of oxygen-containing functional groups and assisting reduction of GO, as shown in the schematic reduction mechanism proposed in Scheme 1. Local high-density energy enables electrical breakdown and discharge at narrow gaps between adjacent GO sheets (Scheme 1a and b). The generated local high temperature can be particularly beneficial to the efficient removal of the functional groups (as shown in Scheme 1a and c). Furthermore, spark impact pressure, together with high-speed ion migration, may also have a deoxygenation effect and contribute to local sheet deformation through striking and sputtering (as depicted in Scheme 1b and d). The generated gaseous products, mainly water vapor and carbon dioxide, escape from GO laminae and lead to further GO expansion and exfoliation (Scheme 1a). As a result, it was observed that the SPSrGO samples had increased in volume during the process of SPS. Unlike conventional thermal reduction processes, SPS is conducted in vacuum, which probably facilitates the escape of those gaseous by-products from GO laminae and thus expedites GO expansion and exfoliation. This is possibly an important reason for the notably high surface area values (up to1265.5 m^2/g) achieved in this study (Scheme 1). Therefore, SPS can be regarded as a multi-functional process that integrates surface roughening into the exfoliation and reduction of GO. In this process, local high temperature, spark impact pressure, and rapid ion migration act in concert and result in hierarchical roughness which can be well maintained during subsequent ultrasonication processes.

Scheme 1. Proposed mechanism for GO reduction by SPS: local high temperature, spark impact pressure and rapid ion migration effectively convert most oxygen-containing functional groups into gaseous products (a and c) and generates lots of hierarchical rough structures on the SPSrGO surface (b and d).

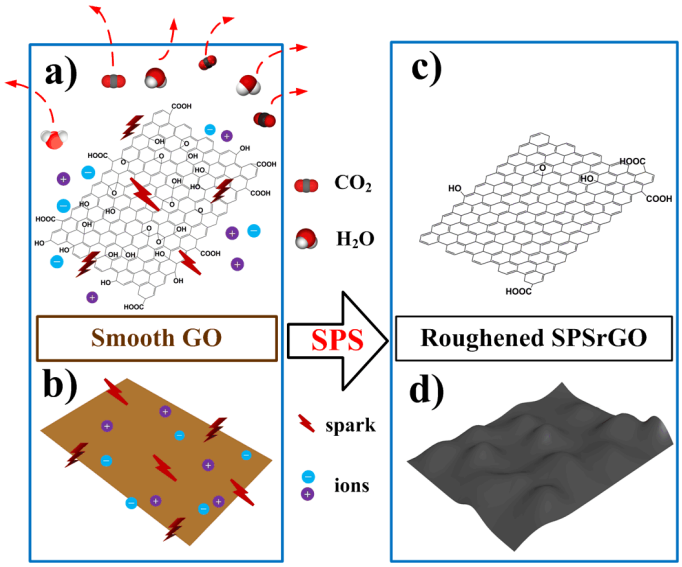

It is believed that the quantity of spark plasma is highest in the early stage of SPS and decreases gradually.[22] Since spark plasma was possibly a significant contributor to GO reduction, cyclic SPS was attempted in hope of achieving a higher degree of reduction by introducing more "early stages". At the SPS temperature of 500 °C, the number of sintering cycles was increased to two (SPSrGO-2C500) and three (SPSrGO-3C500). It was found that the C:O ratio was increased from 9.62 for SPSrGO-500 to 15.13 and 14.90 for SPSrGO-2C500 and SPSrGO-3C500 (Table 1), respectively, corresponding to a much smaller change as compared with that induced by increasing SPS temperature. Furthermore, increasing number of SPS cycles from two to three had virtually no influence on the C:O ratio. Such phenomena can be attributed to several causes. Firstly, a higher temperature may have brought about more intense heating which, as in all other thermal reduction processes, was beneficial for the removal of oxygen-containing

groups. It should be noted that the thermal stability of oxygen containing groups varies (e.g., epoxide < carbonyl < hydroxyl) and a temperature higher than 500 °C is required to remove certain groups.[45] This was probably the reason why extending the holding time at 500 °C from 1 min to 3 min (SPSrGO-500E, Table 1) only achieved a minor increase in C:O ratio (from 9.62 to 11.71, Table 1). In SPS, higher sintering temperatures are realized by exerting a higher voltage and current. This leads to a stronger electric field, higher spark impact pressure and faster ion migration, which possibly further contributed to the removal of the surface functional groups. Secondly, in the later cycle(s) it was likely more difficult to generate spark plasma due to higher vacuum in the chamber. During SPS, the chamber was actively being evacuated, resulting in less and less residual air inside the chamber as the process continued, as confirmed by the increasing vacuum level in the chamber indicated by the Pirani gauge. This weakens the generation of plasma, because the presence of gases is essential for creating plasma. It is worth mentioning that both oxygen-containing groups and intercalated species (mainly water) in GO turned into gaseous products during the reduction process, which could enhance plasma generation. However, their conversion is believed to happen mainly in the early stage of the first SPS cycle, which can be supported by the fact that major weight loss occurred at below 250 °C during the TGA test of GO (Figure S2). The significantly reduced sample resistance and increased electrical conductivity in the first SPS cycle may also have made spark generation more difficult in the subsequent cycles. As shown in Table 1, SPSrGO-500 possessed a buckypaper sheet resistance as low as 12.4 ± 0.8 Ω/sq. As a result, there already existed a highly conductive sponge-like network inside the graphite die during the later SPS cycles which likely facilitated current flow and reduced spark generation.

3.3. Superhydrophobicity. It is believed that both low oxygen content and hierarchical roughness can contribute to the hydrophobicity of SPSrGO,[46] so water contact angles (CAs) were measured on GO and SPSrGO-coated parafilm. It is found that GO possessed a small DI water contact angle of 53.16°, which was smaller than 90° and confirmed its hydrophilicity (Fig. 4a). Reducing GO by SPS at 3 different temperatures significantly increased the DI water contact angle by a factor of two (Fig. 4a), converting it into a highly hydrophobic material. Specially, SPSrGO-1050 showed a DI water contact angle of 153°, indicating that it was superhydrophobic. Using the Young-Dupre's equation,[47] the work of adhesion (W) was calculated for 4 coatings and plotted in Fig. 4a. While W for GO was 116.6 mN/m, SPSrGO-1050 had a W as low as 8.0 mN/m which was two orders of magnitude lower than GO. The significantly decreased W of the SPSrGO-1050 coating could enable very swift movement of liquid droplet on its surface and hence the achievement of a self-cleaning effect. It should be noted that SPSrGO-1050 solution in DMF used for producing the coatings had undergone prolonged ultrasonication which consisted of 10 min bath sonication (550 W) and 5 min horn sonication (130 W). The clearly visible hierarchical rough structures and superhydrophobicity seen in Fig. 4 provide strong evidence for the enduring deformation and roughening effect induced in SPSrGO-1050 during the SPS process. Unlike rGO obtained by conventional thermal reduction,[14] SPSrGO sheets were able to maintain the hierarchical rough structures even after prolonged ultrasonication and thus expected to possess sustained superhydrophobicity over a longer period.

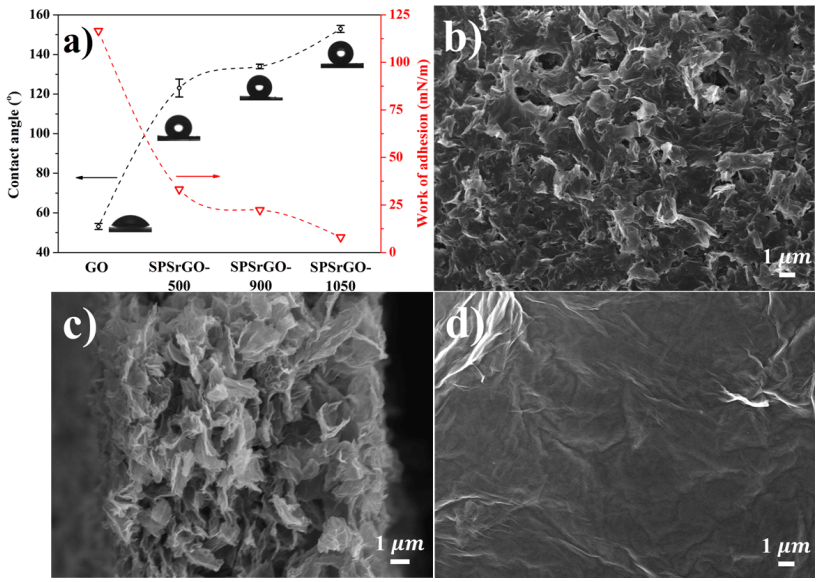

Fig. 4. (a) Water CAs and work of adhesion of GO and SPSrGO coatings, with insets showing a water droplet on different coatings; (b, c) FESEM images of the surface morphology (b) and cross-section (c) of SPSrGO-1050 coating; (d) FESEM image of the GO coating.

The drastically different wettability of GO and SPSrGO can be explained by both morphological and chemical changes with thermal reduction. Compared with the smooth surface of the GO coating (Fig. 4d), SPSrGO-1050 surface possessed lots of hierarchical micro/nano-sized wrinkled structures (Fig. 4b, c) which could trap air and therefore greatly reduce their contact area with the water droplet.[29] The influence of decreased gas-solid interface can be explained by Cassie's model:[48]

$$\cos \theta_r = f(\cos \theta_s + 1) - 1 \quad (1)$$

where f is the fraction of solid contact area, θ_r and θ_s are CAs on the rough and smooth surface, respectively. With the presence of hierarchical roughness, there existed numerous protrusions and peaks on the SPSrGO-1050 coating which prevented the penetration of water into the valleys

between them. Therefore, the water-rGO contact area was significantly reduced and a low f and high θ_r could be obtained. In terms of chemical composition, most hydrophilic functional groups were removed during the SPS process (Fig. 2 and Figure S4), which substantially lowered the surface energy and drastically altered the samples' wettability.

3.4. Bacterial Antifouling and Inactivation Performances. The morphology of *E. coli* after 2 h incubation under aqueous conditions is presented in Fig. 5. As shown in Fig. 5a and b, after 2 h interaction with GO many *E. coli* cells were observed on GO sheets and many of them were either covered or wrapped by GO. This was possibly due to the smooth surface topography and homogeneous dispersion of GO in 0.85% saline solution, both of which contributed to a large contact area between the *E. coli* cells and GO sheets. In the three-step antibacterial mechanism for single walled carbon nanotubes and graphene based materials,[36, 49] cell deposition on the materials is the first step and it can be strongly influenced by the surface functional groups.[37, 50] Because of the presence of a large quantify of oxygen containing functional groups, GO sheets could form stable aqueous dispersions and provide plentiful opportunities for *E. coli* cells to interact with and bind to them.

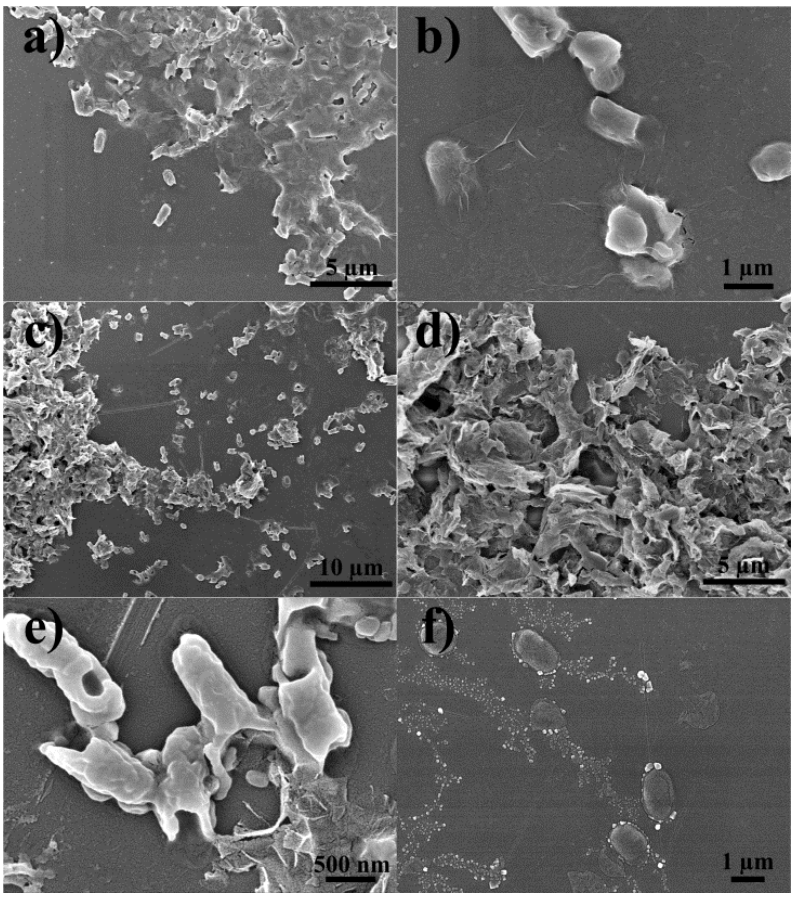

Fig. 5. FESEM images of *E. coli* after 2 h incubation in GO dispersion (a, b), SPSrGO-1050 dispersion (c-e), and pure saline solution (f).

By contrast, almost no *E. coli* cell was found on SPSrGO-1050 (Fig. 5c-e). Those found around the SPSrGO-1050 clusters were probably cells in the 0.85% saline solution introduced in the preparation of the FESEM samples. It was observed that the continuous shaking during the 2 h incubation could prevent the sedimentation of SPSrGO-1050. Therefore, it is believed that the interactions between *E. coli* and suspended SPSrGO could take place at a high rate. However, it seemed to be much harder for *E. coli* cells to adhere onto SPSrGO-1050 compared with GO. This can be ascribed to two possible reasons. Firstly, the superhydrophobicity of SPSrGO-1050 decreased the solid-liquid contact area, which minimized the chances of *E. coli* cells reaching the

SPSrGO sheets. Secondly, for those cells attached to the SPSrGO surface, they could be easily "washed" away by the flowing water due to the weak adhesion strength originating from the limited number of attachment points on the hierarchically rough SPSrGO. Topographically corrugated surfaces have long been regarded as promising antifouling solutions, provided that the surface roughness is smaller than the size of the settling cell.[27] In SPSrGO-1050 numerous protrusions smaller than the length of *E. coli* (~2 μm) were explicitly seen (Fig. 3). Furthermore, the hierarchical roughness could further strengthen the bacterial antifouling efficacy because corrugations in multiple length scales were able to act synergistically to tackle *E. coli* cells in different stages of the cell cycle. Based on the above two reasons, it would be energetically more favorable for *E. coli* cells to stay in 0.85% saline solution rather than to attach onto the SPSrGO-1050 surface.

In addition, compared to *E. coli* cells incubated in pure saline solution (Fig. 5f), cell deformation was clearly observed for those treated by GO or SPSrGO-1050 dispersion. As displayed in Fig. 5b and e, shrinkage of cells could be apparently found, indicating the leakage of intercellular substances. Similar results were also reported by other studies,[36-37, 51-52] where both GO and rGO showed antibacterial effect to some extent. It was proposed in those studies that the inactivation of bacterial cells resulted from the membrane stress caused by the sharp edges and oxidative stress of the nanosheets.[35-36, 49, 51] Generally, the hydrophilic nature enables GO to disperse stably in water, offering it increased possibilities to interact with and thereafter inactivate bacterial cells. On the other hand, rGO was believed to possess a stronger capability to oxidize thiols or other cellular components by virtue of its eminent electrical conductivity, although this effect may be hindered by its poor dispersion in water.[36] In this study, both GO and SPSrGO-1050 were found to be able to inhibit the growth of *E. coli* cells via damaging their

membranes (Fig. 5b and e), which was probably caused by the aforementioned cytotoxicity mechanism in aqueous conditions. It should be pointed out that quite a few conflicting results have been reported with regard to the bacterial inactivation effect of GO and rGO.[36-37, 53] These reports imply that the antibacterial performance of GO and rGO is time and concentration dependent, and higher efficiency may be achieved by applying extended incubation time and/or increased dosage concentration. GO and SPSrGO-1050 coatings were thus fabricated on Teflon filters to interact with *E. coli* cells for a longer incubation period of 18 h.

Figure S9 presents the photos of *E. coli* agar plates after 18 h incubation with uncoated as well as GO and SPSrGO-1050 coated Teflon filters. While clear *E. coli* culture was observed in the areas covered by pure Teflon filter and GO coated filter (Figure S9a, b, d, e), such culture could not be found in the region where SPSrGO-1050 coated filter had been placed (Figure S9c, f). It suggests that *E. coli* cells were able to grow well when in contact with uncoated Teflon and the GO coating while SPSrGO-1050 could effectively inhibit the adhesion and proliferation of *E. coli*.

FESEM was applied to further observe the surface morphology of these filters (Fig. 6). As can be seen from Fig. 6a and b, numerous *E. coli* cells attached tightly on the uncoated Teflon filter. A very similar phenomenon was observed on the filter coated with GO (Fig. 6c and d), indicating that these cells could firmly adhere and vigorously proliferate on the GO coating. Unlike in the saline solution, GO sheets on the surface of Teflon filter were static. This would not only reduce their interactions with *E. coli* cells and mitigate the membrane stress induced by the sharp edges of GO nanosheets, but also lessen the destructive change in membrane permeability caused by the accumulation of GO sheets on the cell surface.[54] As an electrically insulating material, GO has a much weaker oxidation ability than rGO which could further

restrict its inhibition effect on *E. coli* cells.[36] Without strong membrane stress or oxidation stress, *E. coli* cells could readily attach to the GO sheets and actively grow to form colonies.

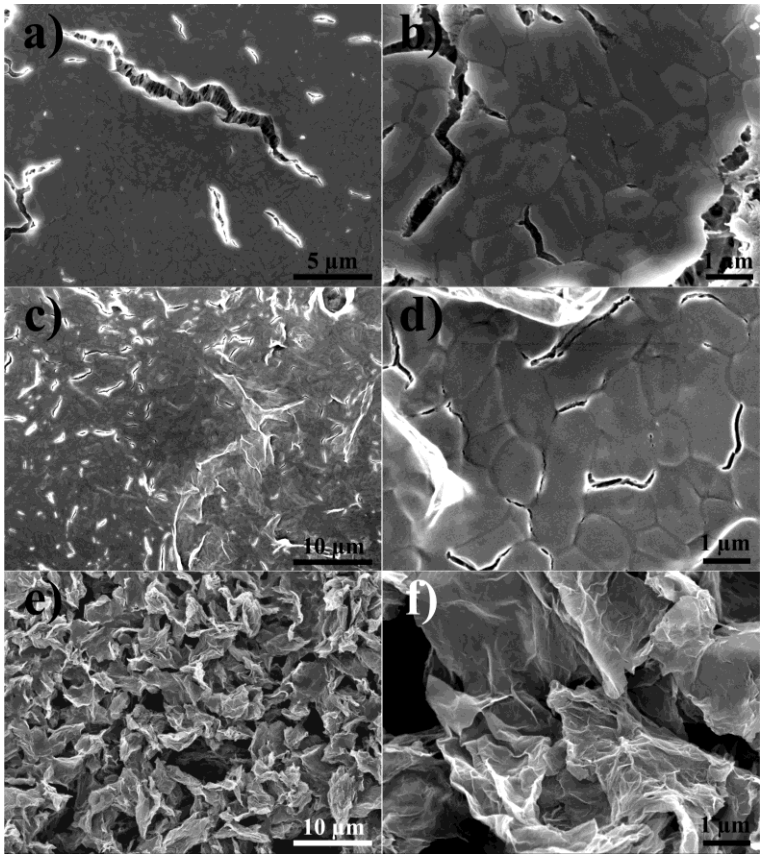

Fig. 6. FESEM images of 3 different Teflon filters placed on agar plate inoculated with *E. coli* for 18 h: (a, b) uncoated, (c, d)GO coated, and (e, f) SPSrGO-1050 coated.

On the contrary, no *E. coli* cell was found on the surface of SPSrGO-1050 coated Teflon filter as displayed in Fig. 6e, f. It signifies that SPSrGO-1050 coating could effectively inhibit the attachment and growth of *E. coli* cells. This may be caused by two major reasons. First, the well retained hierarchical rough structure of SPSrGO-1050 could effectively hinder the adhesion of *E. coli* cells (Fig. 6 e, f). More importantly, the excellent electrical conductivity (Table 1) of SPSrGO-1050 could impose strong oxidation stress on the cells in contact with the SPSrGO

sheets. Under these two stresses, the growth and proliferation of *E. coli* cells would be strongly inhibited or even inactivated. Consequently, no adhesion of cells was spotted on the SPSrGO-1050 coating and no *E. coli* culture formation was observed in the agar plate area underneath the coating. This excellent inactivation effect against *E. coli* implies that it is highly promising to use SPSrGO-1050 to fabricate antibacterial surfaces.

The adhesion and proliferation of bacterial cells on abiotic surfaces can lead to the formation of colonies or even biofilms, which are detrimental to many medical and industrial applications. To date, various strategies have been devised to restrain the colonization of bacteria on material surfaces and a great deal of effort has been devoted to the development of antibacterial materials. In the past few decades, the imprudent and excessive usage of various natural or synthetic biocides has induced various problems such as the emergence of bacterial resistance and potential threats to human health and the environment.[55-56] Considering these issues, enormous attention has been aroused to design antibacterial materials without using any biocide. In our study, the superhydrophobic SPSrGO has demonstrated remarkable bacterial antifouling and inactivation effect both in aqueous solution and as a coating. Therefore, the superhydrophobic SPSrGO fabricated in this study can be a very promising material for achieving long-term antibacterial effect without the addition of any antibacterial agent.

4. CONCLUSIONS

In summary, we demonstrated for the first time a single-step process towards achieving superhydrophobic rGO through SPS. GO could be successfully exfoliated, reduced and hierarchically roughened by SPS at a temperature as low as 500 °C, which is lower than the critical temperature (550 °C) required for GO exfoliation in a conventional thermal process. In addition, SPS demonstrated superior efficacy in minimizing residual oxygen content and creating

surface roughness on both micron and nano-scale. After 1 min of SPS treatment at 1050 °C, the R_a value was increased by a factor of ~10 from GO to SPSrGO. Unlike rGO obtained by conventional thermal reduction, the hierarchical surface roughness in SPSrGO could be well preserved after prolonged ultrasonication. SPSrGO-1050 showed notable electrical conductivity and water CA of 153° as a result of the synergistic effect of local high temperature, spark impact pressure and rapid ion migration. While bacterial attachment on GO was ubiquitously observed in saline solution and solid state, SPSrGO-1050 could effectively prevent the adhesion of *E. coli* cells under both conditions. Although GO and SPSrGO-1050 were both capable of inhibiting the growth of *E. coli* in aqueous conditions to a certain extent, only SPSrGO-1050 coating showed antibacterial effect on *E. coli* cells in the agar plate. We therefore believe that the superhydrophobic SPSrGO is endowed with enormous potential in a wide variety of industrial and biomedical applications.

Furthermore, SPSrGO has great promise to be utilized as a reinforcing agent in metal/ceramic-based composites which can be fabricated by SPS. The current study thus provides valuable insights into the *in situ* reduction and enhancement effects in those composite systems as well.

ASSOCIATED CONTENT

Supporting Information. The Supporting Information is available free of charge on the ACS Publications website at DOI: 10.1021/xxxxxx.

Additional FESEM images; AFM images; comparison of the C:O ratio obtained in this study with those from literature; additional XPS spectra; TGA, FTIR and Raman data; photos of *E. coli* agar plates.

AUTHOR INFORMATION

Corresponding Author

*E-mail: mkakhor@ntu.edu.sg

Notes

The authors declare no competing financial interest.

ACKNOWLEDGMENTS

Z. L. thanks NTU for the University Research Scholarship. Dr. SG Bi, Dr. CH Zhang, Dr. N Li and Dr. H Zhang are gratefully acknowledged for their technical assistance.

REFERENCES

(1) Novoselov, K. S.; Geim, A. K.; Morozov, S.; Jiang, D.; Zhang, Y.; Dubonos, S.; Grigorieva, I.; Firsov, A. Electric Field Effect in Atomically Thin Carbon Films. *Science* **2004,** *306* (5696), 666-669.

(2) Geim, A. K.; Novoselov, K. S. The Rise of Graphene. *Nat. Mater.* **2007,** *6* (3), 183-191.

(3) Lee, C.; Wei, X.; Kysar, J. W.; Hone, J. Measurement of the Elastic Properties and Intrinsic Strength of Monolayer Graphene. *Science* **2008,** *321* (5887), 385-388.

(4) Gao, W.; Alemany, L. B.; Ci, L.; Ajayan, P. M. New Insights into the Structure and Reduction of Graphite Oxide. *Nat. Chem.* **2009,** *1* (5), 403-408.

(5) Dreyer, D. R.; Park, S.; Bielawski, C. W.; Ruoff, R. S. The Chemistry of Graphene Oxide. *Chem. Soc. Rev.* **2010,** *39* (1), 228-240.

(6) Tang, X.-Z.; Cao, Z.; Zhang, H.-B.; Liu, J.; Yu, Z.-Z. Growth of Silver Nanocrystals on Graphene by Simultaneous Reduction of Graphene Oxide and Silver Ions with a Rapid and Efficient One-Step Approach. *Chem. Commun.* **2011,** *47* (11), 3084-3086.

(7) Fan, X. B.; Peng, W. C.; Li, Y.; Li, X. Y.; Wang, S. L.; Zhang, G. L.; Zhang, F. B. Deoxygenation of Exfoliated Graphite Oxide under Alkaline Conditions: A Green Route to Graphene Preparation. *Adv. Mater.* **2008,** *20* (23), 4490-4493.

(8) Larciprete, R.; Fabris, S.; Sun, T.; Lacovig, P.; Baraldi, A.; Lizzit, S. Dual Path Mechanism in the Thermal Reduction of Graphene Oxide. *J. Am. Chem. Soc.* **2011,** *133* (43), 17315-17321.

(9) Sheng, K. X.; Sun, Y. Q.; Li, C.; Yuan, W. J.; Shi, G. Q. Ultrahigh-Rate Supercapacitors Based on Eletrochemically Reduced Graphene Oxide for Ac Line-Filtering. *Sci. Rep.* **2012,** *2*, 1-5.

(10) Zhu, Y. W.; Murali, S.; Cai, W. W.; Li, X. S.; Suk, J. W.; Potts, J. R.; Ruoff, R. S. Graphene and Graphene Oxide: Synthesis, Properties, and Applications. *Adv. Mater.* **2010,** *22* (35), 3906-3924.

(11) Tang, X.-Z.; Li, X.; Cao, Z.; Yang, J.; Wang, H.; Pu, X.; Yu, Z.-Z. Synthesis of Graphene Decorated with Silver Nanoparticles by Simultaneous Reduction of Graphene Oxide and Silver Ions with Glucose. *Carbon* **2013,** *59*, 93-99.

(12) Stankovich, S.; Dikin, D. A.; Dommett, G. H. B.; Kohlhaas, K. M.; Zimney, E. J.; Stach, E. A.; Piner, R. D.; Nguyen, S. B. T.; Ruoff, R. S. Graphene-Based Composite Materials. *Nature* **2006,** *442* (7100), 282-286.

(13) Park, S.; An, J.; Jung, I.; Piner, R. D.; An, S. J.; Li, X.; Velamakanni, A.; Ruoff, R. S. Colloidal Suspensions of Highly Reduced Graphene Oxide in a Wide Variety of Organic Solvents. *Nano Lett.* **2009,** *9* (4), 1593-1597.

(14) McAllister, M. J.; Li, J.-L.; Adamson, D. H.; Schniepp, H. C.; Abdala, A. A.; Liu, J.; Herrera-Alonso, M.; Milius, D. L.; Car, R.; Prud'homme, R. K.; Aksay, I. A. Single Sheet Functionalized Graphene by Oxidation and Thermal Expansion of Graphite. *Chem. Mater.* **2007,** *19* (18), 4396-4404.

(15) Schniepp, H. C.; Li, J.-L.; McAllister, M. J.; Sai, H.; Herrera-Alonso, M.; Adamson, D. H.; Prud'homme, R. K.; Car, R.; Saville, D. A.; Aksay, I. A. Functionalized Single Graphene Sheets Derived from Splitting Graphite Oxide. *J. Phys. Chem. B* **2006,** *110* (17), 8535-8539.

(16) Gu, Y. W.; Loh, N. H.; Khor, K. A.; Tor, S. B.; Cheang, P. Spark Plasma Sintering of Hydroxyapatite Powders. *Biomaterials* **2002,** *23* (1), 37-43.

(17) Meng, J.; Loh, N. H.; Tay, B. Y.; Tor, S. B.; Fu, G.; Khor, K. A.; Yu, L. Pressureless Spark Plasma Sintering of Alumina Micro-Channel Part Produced by Micro Powder Injection Molding. *Scripta Mater.* **2011,** *64* (3), 237-240.

(18) Huang, M.; Li, Z.; Wu, J.; Khor, K. A.; Huo, F.; Duan, F.; Lim, S. C.; Yip, M. S.; Yang, J. Multifunctional Alumina Composites with Toughening and Crack ‐ Healing Features via Incorporation of Nial Particles. *J. Am. Ceram. Soc.* **2015,** *98* (5), 1618-1625.

(19) Munir, Z.; Anselmi-Tamburini, U.; Ohyanagi, M. The Effect of Electric Field and Pressure on the Synthesis and Consolidation of Materials: A Review of the Spark Plasma Sintering Method. *J. Mater. Sci.* **2006,** *41* (3), 763-777.

(20) Garay, J. E. Current-Activated, Pressure-Assisted Densification of Materials. *Annu. Rev. Mater. Res.* **2010,** *40*, 445-468.

(21) Munir, Z. A.; Quach, D. V.; Ohyanagi, M. Electric Current Activation of Sintering: A Review of the Pulsed Electric Current Sintering Process. *J. Am. Ceram. Soc.* **2011,** *94* (1), 1-19.

(22) Omori, M. Sintering, Consolidation, Reaction and Crystal Growth by the Spark Plasma System (SPS). *Mater. Sci. Eng. A* **2000,** *287* (2), 183-188.

(23) Porwal, H.; Grasso, S.; Mani, M. K.; Reece, M. J. In Situ Reduction of Graphene Oxide Nanoplatelet During Spark Plasma Sintering of a Silica Matrix Composite. *J. Eur. Ceram. Soc.* **2014,** *34* (14), 3357-3364.

(24) Ramírez, C.; Vega-Diaz, S. M.; Morelos-Gómez, A.; Figueiredo, F. M.; Terrones, M.; Osendi, M. I.; Belmonte, M.; Miranzo, P. Synthesis of Conducting Graphene/Si_3n_4 Composites by Spark Plasma Sintering. *Carbon* **2013,** *57* (0), 425-432.

(25) Ramirez, C.; Miranzo, P.; Belmonte, M.; Osendi, M. I.; Poza, P.; Vega-Diaz, S. M.; Terrones, M. Extraordinary Toughening Enhancement and Flexural Strength in Si3n4 Composites Using Graphene Sheets. *J. Eur. Ceram. Soc.* **2014,** *34* (2), 161-169.

(26) Chen, Z.; Dong, L.; Yang, D.; Lu, H. Superhydrophobic Graphene-Based Materials: Surface Construction and Functional Applications. *Adv. Mater.* **2013,** *25* (37), 5352-5359.

(27) Genzer, J.; Efimenko, K. Recent Developments in Superhydrophobic Surfaces and Their Relevance to Marine Fouling: A Review. *Biofouling* **2006,** *22* (5), 339-360.

(28) Lin, Y.; Ehlert, G. J.; Bukowsky, C.; Sodano, H. A. Superhydrophobic Functionalized Graphene Aerogels. *ACS Appl. Mater. Interfaces* **2011,** *3* (7), 2200-2203.

(29) Liu, Q.; Chen, D. X.; Kang, Z. X. One-Step Electrodeposition Process to Fabricate Corrosion-Resistant Superhydrophobic Surface on Magnesium Alloy. *ACS Appl. Mater. Interfaces* **2015,** *7* (3), 1859-1867.

(30) Wang, J.-N.; Shao, R.-Q.; Zhang, Y.-L.; Guo, L.; Jiang, H.-B.; Lu, D.-X.; Sun, H.-B. Biomimetic Graphene Surfaces with Superhydrophobicity and Iridescence. *Chem. Asian J.* **2012,** *7* (2), 301-304.

(31) Singh, E.; Chen, Z.; Houshmand, F.; Ren, W.; Peles, Y.; Cheng, H.-M.; Koratkar, N. Superhydrophobic Graphene Foams. *Small* **2013,** *9* (1), 75-80.

(32) Banerjee, I.; Pangule, R. C.; Kane, R. S. Antifouling Coatings: Recent Developments in the Design of Surfaces That Prevent Fouling by Proteins, Bacteria, and Marine Organisms. *Adv. Mater.* **2011,** *23* (6), 690-718.

(33) Privett, B. J.; Youn, J.; Hong, S. A.; Lee, J.; Han, J.; Shin, J. H.; Schoenfisch, M. H. Antibacterial Fluorinated Silica Colloid Superhydrophobic Surfaces. *Langmuir* **2011,** *27* (15), 9597-9601.

(34) Crick, C. R.; Ismail, S.; Pratten, J.; Parkin, I. P. An Investigation into Bacterial Attachment to an Elastomeric Superhydrophobic Surface Prepared Via Aerosol Assisted Deposition. *Thin Solid Films* **2011,** *519* (11), 3722-3727.

(35) Akhavan, O.; Ghaderi, E. Toxicity of Graphene and Graphene Oxide Nanowalls against Bacteria. *ACS nano* **2010,** *4* (10), 5731-5736.

(36) Liu, S.; Zeng, T. H.; Hofmann, M.; Burcombe, E.; Wei, J.; Jiang, R.; Kong, J.; Chen, Y. Antibacterial Activity of Graphite, Graphite Oxide, Graphene Oxide, and Reduced Graphene Oxide: Membrane and Oxidative Stress. *Acs Nano* **2011,** *5* (9), 6971-6980.

(37) Hu, W.; Peng, C.; Luo, W.; Lv, M.; Li, X.; Li, D.; Huang, Q.; Fan, C. Graphene-Based Antibacterial Paper. *Acs Nano* **2010,** *4* (7), 4317-4323.

(38) Hummers, W. S.; Offeman, R. E. Preparation of Graphitic Oxide. *J. Am. Chem. Soc.* **1958,** *80* (6), 1339-1339.

(39) Tang, X.-Z.; Li, W.; Yu, Z.-Z.; Rafiee, M. A.; Rafiee, J.; Yavari, F.; Koratkar, N. Enhanced Thermal Stability in Graphene Oxide Covalently Functionalized with 2-Amino-4,6-Didodecylamino-1,3,5-Triazine. *Carbon* **2011,** *49* (4), 1258-1265.

(40) Song, N.-J.; Chen, C.-M.; Lu, C. X.; Liu, Z.; Kong, Q.-Q.; Cai, R. Thermally Reduced Graphene Oxide Films as Flexible Lateral Heat Spreaders. *J. Mater. Chem. A* **2014,** *2* (39), 16563-16568.

(41) Cote, L. J.; Cruz-Silva, R.; Huang, J. Flash Reduction and Patterning of Graphite Oxide and Its Polymer Composite. *J. Am. Chem. Soc.* **2009,** *131* (31), 11027-11032.

(42) Tokita, M., Mechanism of Spark Plasma Sintering. In *Proceeding of the International Symposium on Microwave, Plasma and Thermochemical Processing of Advanced Materials*, Miyake, S.; Samandi, M., Eds. Osaka Japan, JWRI Osaka University, **1997**; pp 69-76.

(43) Yu, L. G.; Khor, K. A.; Li, H.; Cheang, P. Effect of Spark Plasma Sintering on the Microstructure and in Vitro Behavior of Plasma Sprayed Ha Coatings. *Biomaterials* **2003,** *24* (16), 2695-2705.

(44) Cao, B.; Yu, G. N.; Pan, C. X. The Ripple's Enhancement in Graphene Sheets by Spark Plasma Sintering. *AIP Adv.* **2011,** *1* (3), 032170-032170-6.

(45) Wang, D.-W.; Du, A.; Taran, E.; Lu, G. Q.; Gentle, I. R. A Water-Dielectric Capacitor Using Hydrated Graphene Oxide Film. *J. Mater. Chem.* **2012,** *22* (39), 21085-21091.

(46) Liu, K.; Jiang, L. Bio-Inspired Self-Cleaning Surfaces. *Annu. Rev. Mater. Res.* **2012,** *42*, 231-263.

(47) Nosonovsky, M.; Bhushan, B. Multiscale Friction Mechanisms and Hierarchical Surfaces in Nano-and Bio-Tribology. *Mater. Sci. Eng. R* **2007,** *58* (3), 162-193.

(48) Cassie, A. B. D.; Baxter, S. Wettability of Porous Surfaces. *Trans. Faraday Soc.* **1944,** *40* (0), 546-551.

(49) Vecitis, C. D.; Zodrow, K. R.; Kang, S.; Elimelech, M. Electronic-Structure-Dependent Bacterial Cytotoxicity of Single-Walled Carbon Nanotubes. *ACS nano* **2010,** *4* (9), 5471-5479.

(50) Tang, Y. J.; Ashcroft, J. M.; Chen, D.; Min, G.; Kim, C.-H.; Murkhejee, B.; Larabell, C.; Keasling, J. D.; Chen, F. F. Charge-Associated Effects of Fullerene Derivatives on Microbial Structural Integrity and Central Metabolism. *Nano Lett.* **2007,** *7* (3), 754-760.

(51) Hu, W.; Peng, C.; Lv, M.; Li, X.; Zhang, Y.; Chen, N.; Fan, C.; Huang, Q. Protein Corona-Mediated Mitigation of Cytotoxicity of Graphene Oxide. *Acs Nano* **2011,** *5* (5), 3693-3700.

(52) Cai, X.; Tan, S.; Lin, M.; Xie, A.; Mai, W.; Zhang, X.; Lin, Z.; Wu, T.; Liu, Y. Synergistic Antibacterial Brilliant Blue/Reduced Graphene Oxide/Quaternary Phosphonium Salt Composite with Excellent Water Solubility and Specific Targeting Capability. *Langmuir* **2011,** *27* (12), 7828-7835.

(53) Ruiz, O. N.; Fernando, K. S.; Wang, B.; Brown, N. A.; Luo, P. G.; McNamara, N. D.; Vangsness, M.; Sun, Y.-P.; Bunker, C. E. Graphene Oxide: A Nonspecific Enhancer of Cellular Growth. *ACS nano* **2011,** *5* (10), 8100-8107.

(54) Zhou, Y.; Yang, J.; He, T.; Shi, H.; Cheng, X.; Lu, Y. Highly Stable and Dispersive Silver Nanoparticle–Graphene Composites by a Simple and Low-Energy-Consuming Approach and Their Antimicrobial Activity. *Small* **2013,** *9* (20), 3445-3454.

(55) Poole, K. Mechanisms of Bacterial Biocide and Antibiotic Resistance. *J. Appl. Microbiol.* **2002,** *92* (s1), 55S-64S.

(56) Gupta, A.; Silver, S. Molecular Genetics: Silver as a Biocide: Will Resistance Become a Problem? *Nat. Biotechnol.* **1998,** *16* (10), 888-888.

Table of Contents Graphic:

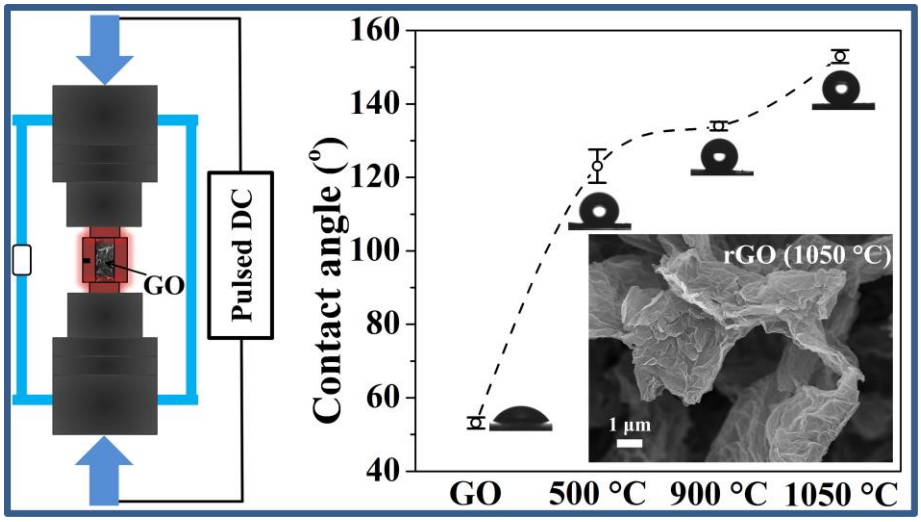

Supporting Information

Single-Step Process toward Achieving Superhydrophobic Reduced Graphene Oxide

Zhong Li,[†] Xiu-Zhi Tang,[†] Wenyu Zhu,[‡] Brianna C. Thompson,[†] Mingyue Huang,[†] Jinglei Yang,[†] Xiao Hu,[§] and Khiam Aik Khor [, †]*

[†]School of Mechanical & Aerospace Engineering, [‡]School of Civil & Environmental Engineering, and [§]School of Materials Science & Engineering, Nanyang Technological University, 50 Nanyang Avenue, Singapore 639798

E-mail: mkakhor@ntu.edu.sg.

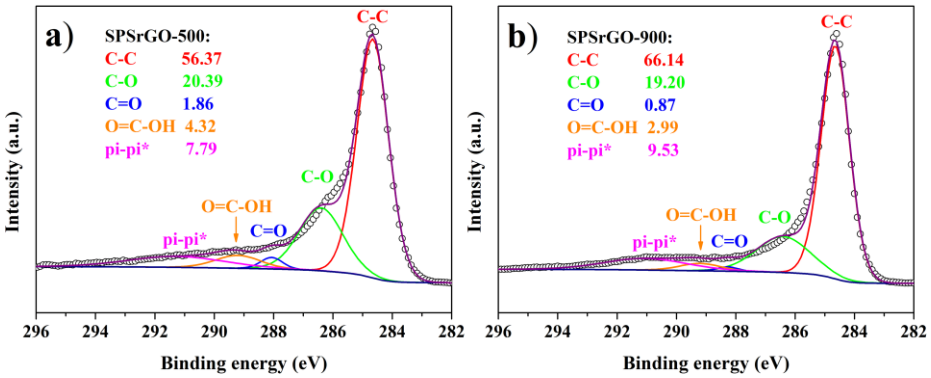

Figure S1. XPS C 1s spectrum of SPSrGO-500 (a) and SPSrGO-900 (b).

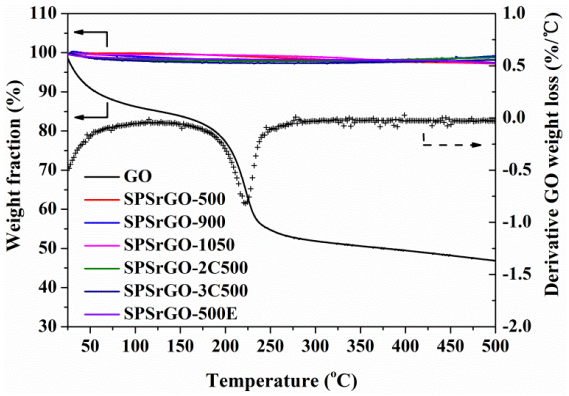

Figure S2. TGA curves of GO and SPSrGO.

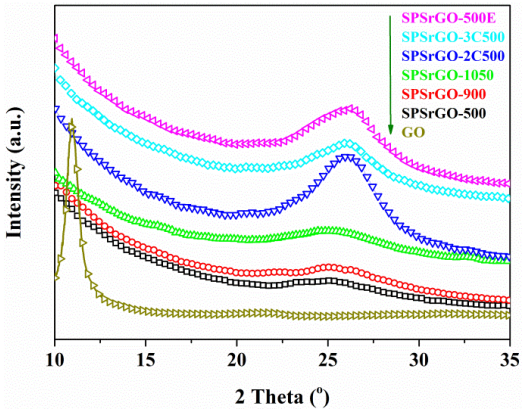

Figure S3. XRD patterns of GO and SPSrGO.

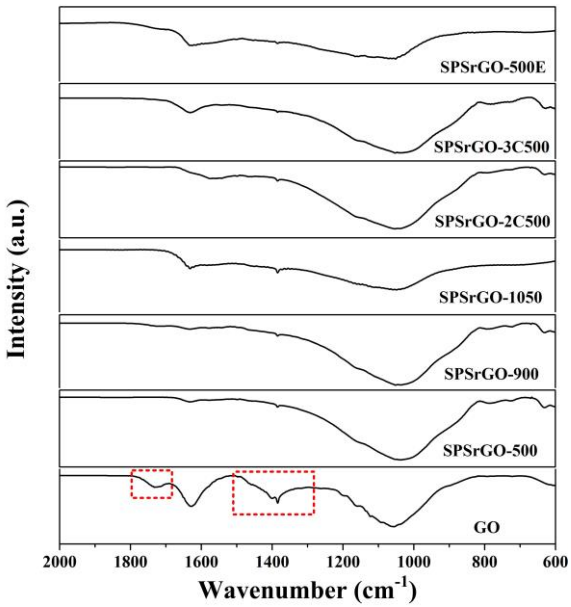

Figure S4. FTIR spectra of GO and SPSrGO.

Note the obviously decreased intensity of the two peaks in red rectangles for SPSrGO. Figure S4 shows four major absorption peaks in the FTIR spectrum of GO centered at 1730, 1625, 1380, and 1070 cm^{-1}, which can be attributed to C=O carboxyl/carbonyl, aromatic C=C, C-O epoxy, and C-O alkoxy, respectively.[1-2]

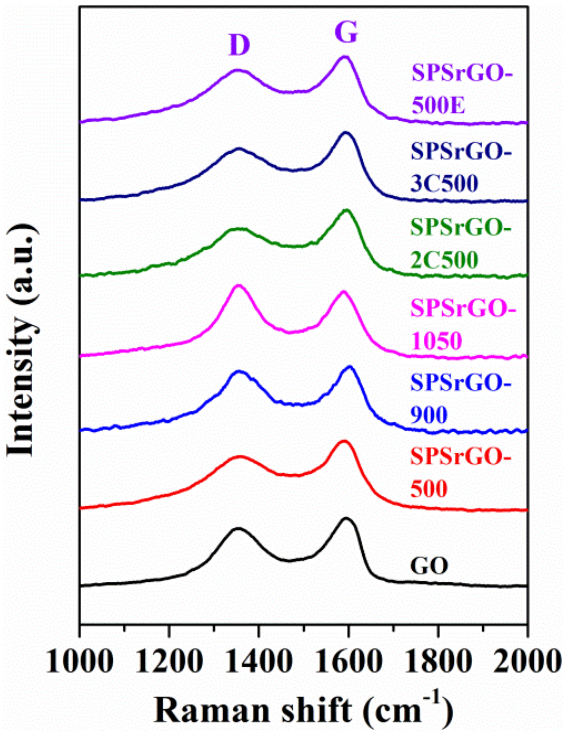

Figure S5. Raman spectra of GO and SPSrGO.

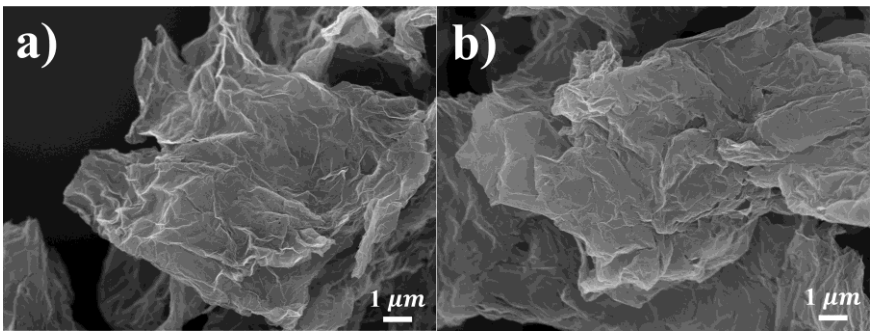

Figure S6. FESEM images of a) SPSrGO-500 and b) SPSrGO-900 cast from a dispersion in ethanol.

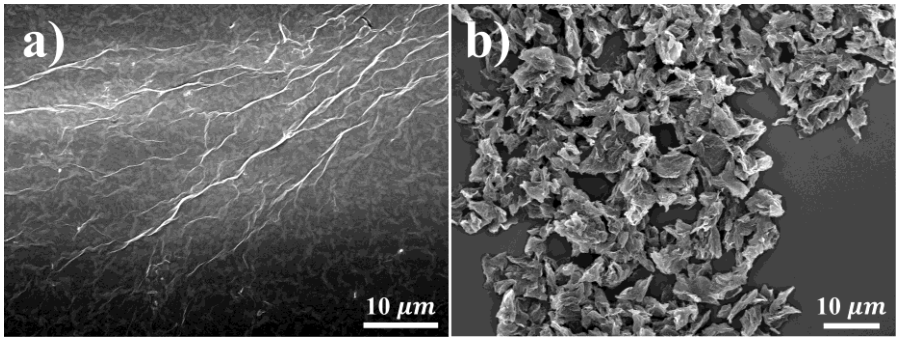

Figure S7. FESEM images of a) GO and b) SPSrGO-1050 cast from a dispersion in water.

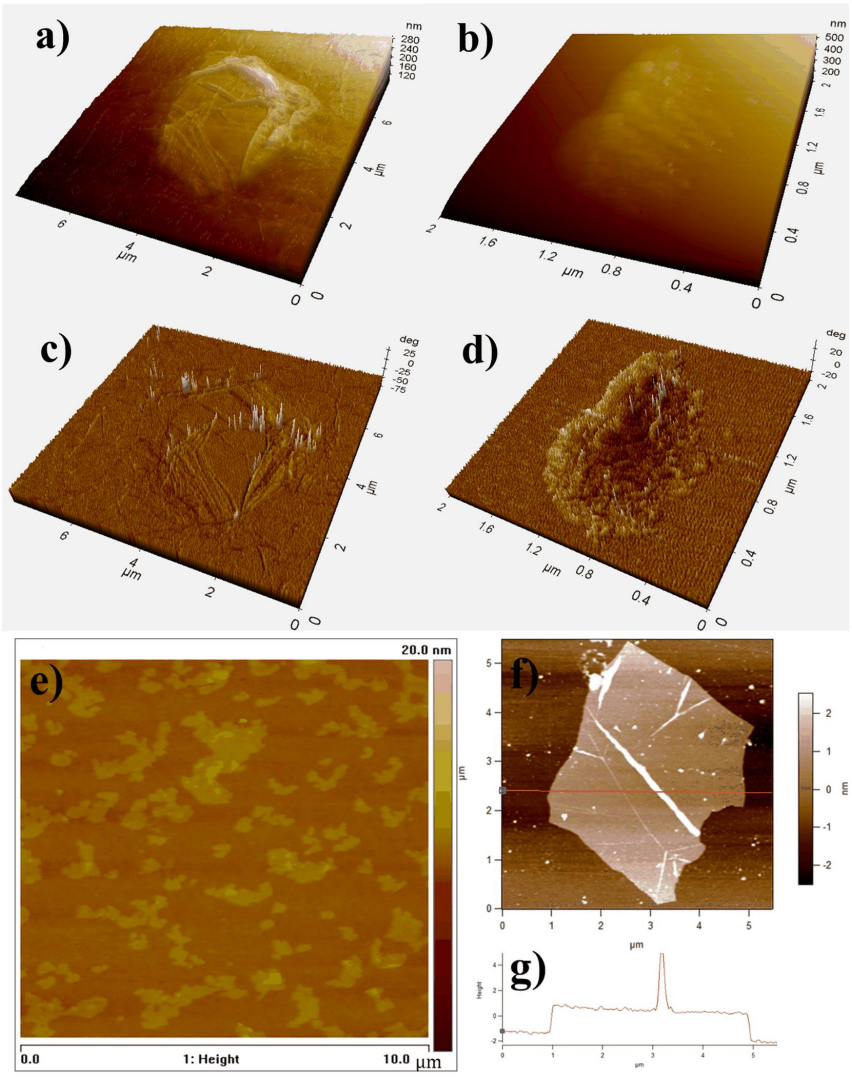

Figure S8. AFM images of GO cast from a dispersion in water (a, c, and e-g) and SPSrGO-1050 cast from a dispersion in DMF (b, d). (a, b) 3D topography images; (c, d) 3D phase images; (e, f) 2D topography images; (g) height profile of a GO sheet in f). Note that different GO concentrations were used for samples in (a, c) and (e, f).

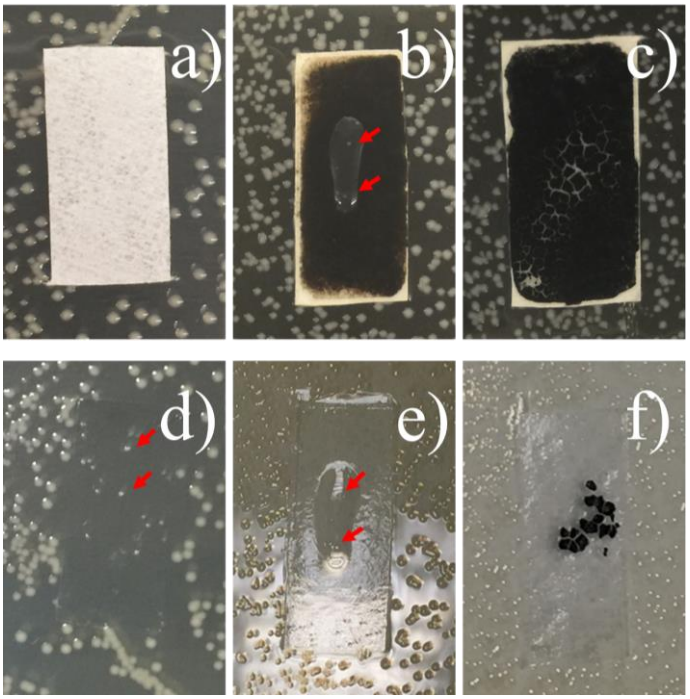

Figure S9. Photos of *E. coli* agar plates covered by uncoated (a), GO-coated (b), and SPSrGO-coated (c) Teflon filters after 18 h incubation; photos of the same agar plates after removing uncoated (d), GO-coated (e), and SPSrGO-coated (f) Teflon filters.

Table S1. Comparison of properties between SPSrGO and other thermally reduced GO

references	method	C:O ratio (by atom %)	BET surface area (m^2/g)	interlamellar spacing (Å)	I_D/I_G ratio	electrical conductivity (S/m)
Current study	SPS at 1050 °C for 1 min	83.03	859	3.57	1.05	1564 (900 °C) [a]
[3]	Annealing at 1200 °C in Ar for 30 min	50.55	Not available	3.44	1.06	Not available
[4]	Microwave treatment at 800 W for 10 min	5.46	Not available	Not available	0.96	200
[5-6]	Held in Ar atmosphere at 1050 °C for 30 s	9.75	600-1500	Not available	Not available	1000-2300
[7]	Flash reduction	4.23	Not available	Not available	Not available	~1000
[8]	Microwave treatment in air at 700 W for 1 min	2.75	463	3.6	Not available	274

[a] Sheet thickness was measured to be 362 μm. Conductivity was calculated by 1/(sheet resistance × thickness).

REFERENCES

(1) Zhang, H.; Hines, D.; Akins, D. L. Synthesis of a Nanocomposite Composed of Reduced Graphene Oxide and Gold Nanoparticles. *Dalton Trans.* **2014,** *43* (6), 2670-2675.

(2) Li, M.; Huang, X. Y.; Wu, C.; Xu, H. P.; Jiang, P. K.; Tanaka, T. Fabrication of Two-Dimensional Hybrid Sheets by Decorating Insulating Pani on Reduced Graphene Oxide for Polymer Nanocomposites with Low Dielectric Loss and High Dielectric Constant. *J. Mater. Chem.* **2012,** *22* (44), 23477-23484.

(3) Song, N.-J.; Chen, C.-M.; Lu, C. X.; Liu, Z.; Kong, Q.-Q.; Cai, R. Thermally Reduced Graphene Oxide Films as Flexible Lateral Heat Spreaders. *J. Mater. Chem. A* **2014,** *2* (39), 16563-16568.

(4) Chen, W. F.; Yan, L. F.; Bangal, P. R. Preparation of Graphene by the Rapid and Mild Thermal Reduction of Graphene Oxide Induced by Microwaves. *Carbon* **2010,** *48* (4), 1146-1152.

(5) McAllister, M. J.; Li, J.-L.; Adamson, D. H.; Schniepp, H. C.; Abdala, A. A.; Liu, J.; Herrera-Alonso, M.; Milius, D. L.; Car, R.; Prud'homme, R. K.; Aksay, I. A. Single Sheet Functionalized Graphene by Oxidation and Thermal Expansion of Graphite. *Chem. Mater.* **2007,** *19* (18), 4396-4404.

(6) Schniepp, H. C.; Li, J.-L.; McAllister, M. J.; Sai, H.; Herrera-Alonso, M.; Adamson, D. H.; Prud'homme, R. K.; Car, R.; Saville, D. A.; Aksay, I. A. Functionalized Single Graphene Sheets Derived from Splitting Graphite Oxide. *J. Phys. Chem. B* **2006,** *110* (17), 8535-8539.

(7) Cote, L. J.; Cruz-Silva, R.; Huang, J. Flash Reduction and Patterning of Graphite Oxide and Its Polymer Composite. *J. Am. Chem. Soc.* **2009,** *131* (31), 11027-11032.

(8) Zhu, Y. W.; Murali, S.; Stoller, M. D.; Velamakanni, A.; Piner, R. D.; Ruoff, R. S. Microwave Assisted Exfoliation and Reduction of Graphite Oxide for Ultracapacitors. *Carbon* **2010,** *48* (7), 2118-2122.